TPC2 mediates new mechanisms of platelet dense granule membrane dynamics through regulation of Ca^{2+} release

Andrea L. Ambrosio, Judith A. Boyle, and Santiago M. Di Pietro
Department of Biochemistry and Molecular Biology, Colorado State University, Fort Collins, CO 80523-1870

ABSTRACT **Platelet dense granules (PDGs) are acidic calcium stores essential for normal hemostasis. They develop from late endosomal compartments upon receiving PDG-specific proteins through vesicular trafficking, but their maturation process is not well understood. Here we show that two-pore channel 2 (TPC2) is a component of the PDG membrane that regulates PDG luminal pH and the pool of releasable Ca^{2+}. Using a genetically encoded Ca^{2+} biosensor and a pore mutant TPC2, we establish the function of TPC2 in Ca^{2+} release from PDGs and the formation of perigranular Ca^{2+} nanodomains. For the first time, Ca^{2+} spikes around PDGs—or any organelle of the endolysosome family—are visualized in real time and revealed to precisely mark organelle "kiss-and-run" events. Further, the presence of membranous tubules transiently connecting PDGs is revealed and shown to be dramatically enhanced by TPC2 in a mechanism that requires ion flux through TPC2. "Kiss-and-run" events and tubule connections mediate transfer of membrane proteins and luminal content between PDGs. The results show that PDGs use previously unknown mechanisms of membrane dynamics and content exchange that are regulated by TPC2.**

Monitoring Editor
Thomas F. J. Martin
University of Wisconsin

Received: Feb 2, 2015
Revised: Jun 17, 2015
Accepted: Jul 15, 2015

INTRODUCTION

Platelet function depends on the release of molecules from membrane-bound compartments known as dense granules and α-granules (Ren *et al.*, 2008; Broos *et al.*, 2011; Thon and Italiano, 2012). Platelet dense granules (PDGs) are important for hemostasis, given the bleeding disorders associated with PDG biogenesis defects, such as those observed in various forms of Hermansky–Pudlak syndrome (McNicol and Israels, 1999; Huizing *et al.*, 2008; Graham *et al.*, 2009). PDG biogenesis and secretion have also been identified as targets for antithrombotic drugs (Graham *et al.*, 2009). Despite the importance of PDGs in hemostasis and thrombosis, their biogenesis is not well understood.

PDGs are lysosome-related organelles with a luminal pH of 5.4 that contain serotonin, ADP, ATP, polyphosphates, and Ca^{2+} (Holmsen and Weiss, 1979; Carty *et al.*, 1981; Flaumenhaft, 2012). PDGs are synthesized in bone marrow megakaryocytes (MKs). They develop from late endosomes/multivesicular bodies, at least in part by receiving newly synthesized membrane proteins through vesicular trafficking (Youssefian and Cramer, 2000; Ambrosio *et al.*, 2012; Meng *et al.*, 2012). The biogenesis of PDGs appears to use components of the ubiquitous integral membrane protein transport machinery, as well as cell type–specific components. Adaptor Protein-3 and Rab38 are examples of the ubiquitous and cell type–specific transport machinery, respectively, that, when mutated, cause PDG deficiency (Huizing *et al.*, 2008). Similarly, the PDG limiting membrane is believed to share some proteins with organelles of the endolysosomal system, as well as to have PDG-specific proteins. LAMP2 and the serotonin transporter VMAT2 are examples of shared and PDG-specific integral membrane proteins, respectively (Ambrosio *et al.*, 2012). Understanding PDG membrane protein composition and function is of fundamental importance because they determine the luminal content and physiology of PDGs. However, our knowledge of PDG membrane protein composition, dynamics, and regulation is in its infancy.

This article was published online ahead of print in MBoC in Press (http://www.molbiolcell.org/cgi/doi/10.1091/mbc.E15-01-0058) on July 22, 2015.

Address correspondence to: Santiago M. Di Pietro (santiago.dipietro@colostate.edu).

Abbreviations used: EGFP, enhanced GFP; GFP, green fluorescent protein; iRFP, infrared fluorescent protein; MK, tmegakaryocyte; MOC, Manders' overlap coefficient; mRFP, monomeric red fluorescent protein; NAADP, nicotinic acid adenine dinucleotide phosphate; PAGFP, photoactivatable GFP; PDG, platelet dense granule; siRNA, small interfering RNA; SNARE, soluble *N*-ethylmaleimide–sensitive factor attachment protein receptor; tfLAMP2, tandem-fluorescence LAMP2; TPC, two-pore channel.

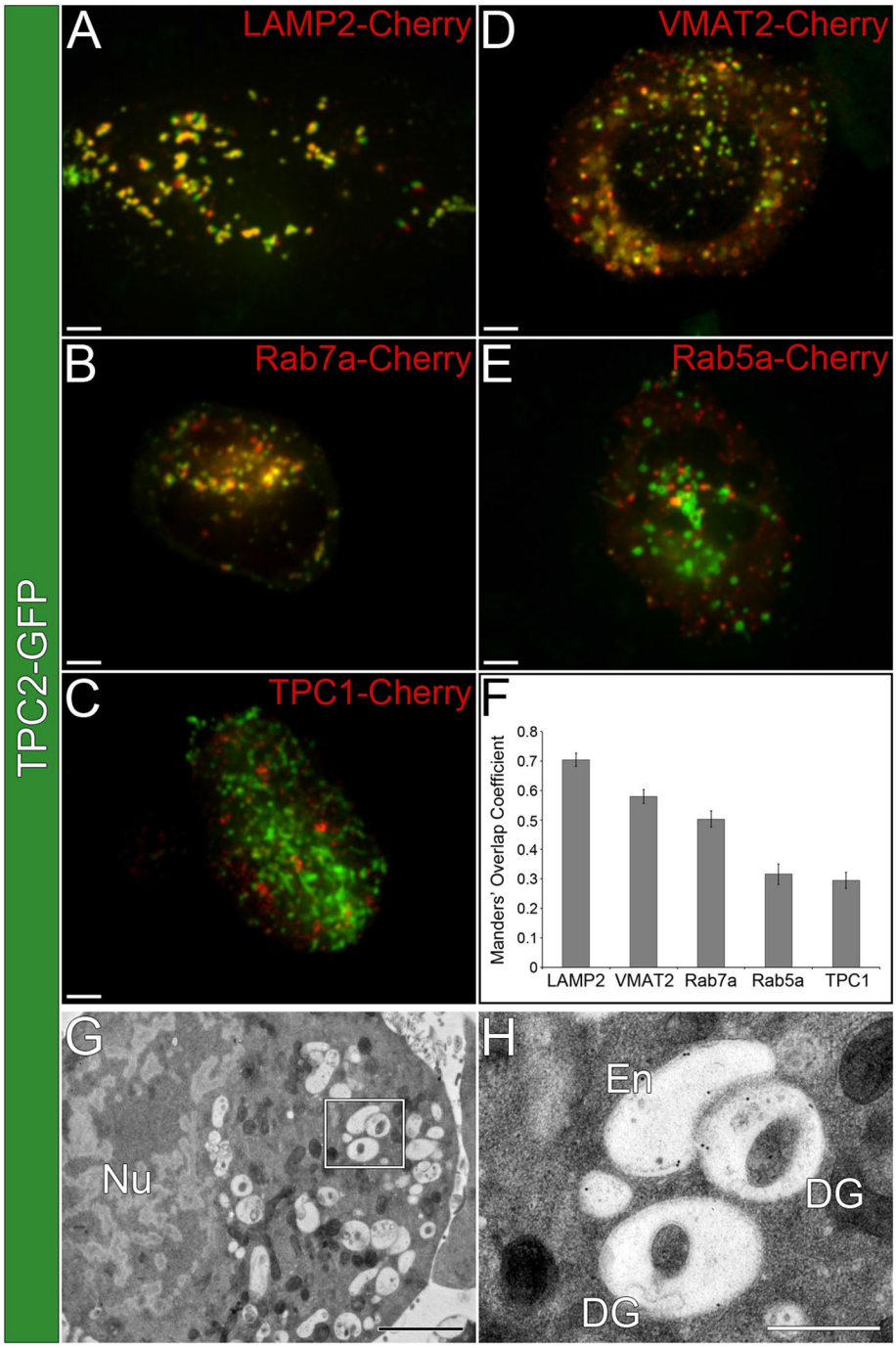

FIGURE 1: TPC2 localizes to PDGs in MEG-01 cells. (A–E) Spinning-disk confocal fluorescence microscopy images of live MEG-01 cells coexpressing TPC2-GFP and (A) LAMP2-Cherry, (B) Rab7a-Cherry, (C) TPC1-Cherry, (D) VMAT2-Cherry, and (E) Rab5a-Cherry. Bars, 5 μm. (F) MOCs were determined for the colocalization between TPC2-GFP and the Cherry-tagged markers described for A–E ($n \geq 10$ cells/treatment). (G) Thin-section immunogold electron micrograph of a MEG-01 cell expressing TPC2-GFP and labeled with an anti-GFP antibody (2200×). Bar, 2 μm. See also Supplemental Figure S1. (H) Higher-magnification view from the region indicated in G showing examples of mature PDGs (DG) and endosomes (En; 8900×). Bar, 500 nm.

Two-pore channel 1 (TPC1) and TPC2 are cation release channels expressed in some acidic calcium stores (Grimm *et al.*, 2012; Morgan and Galione, 2014). In nonspecialized cells, TPC1 and TPC2 are mostly distributed along the endolysosomal system, with TPC1 preferentially expressed in endosomes and TPC2 in the most acidic organelles (Zhu *et al.*, 2010). TPC2 is believed to be a Ca^{2+} channel gated by NAADP, the most potent Ca^{2+} mobilizer (Calcraft *et al.*, 2009). It is unclear whether TPC2 is present and what function it might serve in PDGs.

Here we determine the presence of TPC2 in PDGs by microscopy and biochemical approaches. Using genetically encoded Ca^{2+} and pH biosensors, we demonstrate TPC2 promotes Ca^{2+} release and through this activity regulates the luminal pH of PDGs. TPC2 mediates the formation of perigranular Ca^{2+} nanodomains that exquisitely mark organelle "kiss-and-run" events and promote tubular connections between PDGs. "Kiss-and-run" events and tubules mediate material transfer between PDGs. The data suggest that TPC2 is a new player in PDG maturation and function.

RESULTS

TPC2 is a component of the PDG limiting membrane

To investigate TPC2 localization in PDG-producing cells, we first used a human megakaryocytic cell line, MEG-01, which we established as a faithful model system in which to study PDGs (Ambrosio *et al.*, 2012). MEG-01 cells were cotransfected with a TPC2–green fluorescent protein (GFP) construct and Cherry-tagged markers of PDGs, late endosomes/immature PDGs, and early endosomes (Figure 1, A–F). Live-cell confocal fluorescence microscopy analysis showed a high degree of TPC2 colocalization with markers of PDGs, LAMP2 and VMAT2 (Manders' overlap coefficient [MOC] = 0.70 ± 0.02 and 0.58 ± 0.02, respectively), and late endosomes/immature PDGs, Rab7a (MOC = 0.50 ± 0.03). Early endosome markers Rab5a and TPC1 showed significantly lower colocalization with TPC2 (MOC = 0.32 ± 0.04 and 0.29 ± 0.03, respectively). Control experiments showed that the empirical maximum colocalization MOC detectable for the same marker labeled with two different fluorophores is 0.72 ± 0.02, and MOC values >0.18 ± 0.01 indicate colocalization above background (Ambrosio *et al.*, 2012). Therefore TPC2 is mostly present in PDGs and late endosomes/immature PDGs. Thin-section immunogold electron microscopy analysis of MEG-01 cells expressing TPC2-GFP and labeled with an anti-GFP antibody also showed that the exogenous protein localizes to PDGs and late endosomes/immature PDGs (81% of the label, 423 gold particles, 19 cells; Figure 1, G and H, and Supplemental Figure S1). Immature PDGs can be distinguished from mature PDGs by their lower amount of internal dense material.

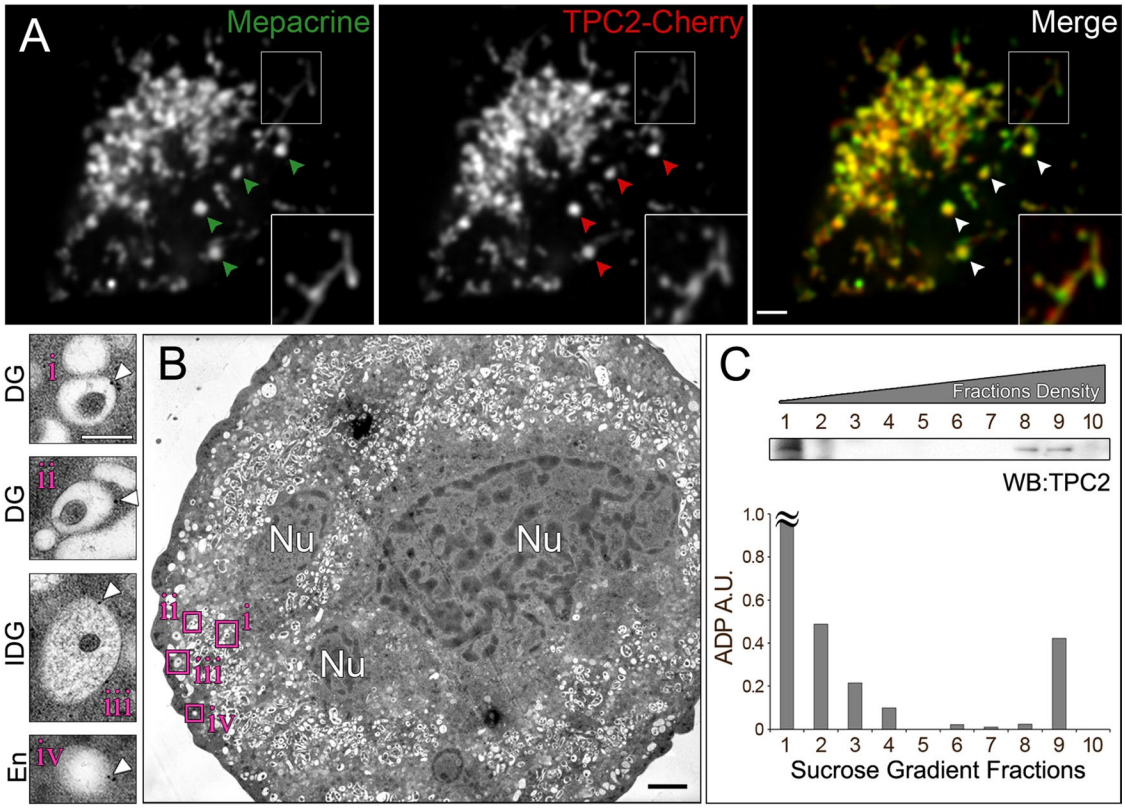

FIGURE 2: TPC2 localizes to PDGs in primary MKs. (A) Spinning-disk confocal fluorescence microscopy images of a live primary bone marrow MK expressing TPC2-Cherry and incubated with the PDG-specific green fluorescent dye mepacrine. Bar, 5 µm. Inset, magnified view of the indicated region showing PDGs connected by tubules. (B) Thin-section immunogold electron micrograph of a primary MK labeled with the chicken TPC2-C antibody (7000×). Insets (15,000×), examples of mature PDGs (i, ii), immature PDG (iii), and endosome (iv). White arrowheads indicate gold particles. Black bar, 2 µm; white bar, 250 nm. Nu, nucleus. See also Supplemental Figure S3. (C) Subcellular fractionation of primary MKs. The postnuclear supernatant of a primary MK extract was subjected to a 10–60% linear sucrose gradient fractionation. Fractions obtained were analyzed for their ADP content and immunoblotting with a rabbit anti-TPC2 antibody. ≈, out of scale.

To corroborate the localization of TPC2 to PDGs, we isolated primary MKs from mouse bone marrow and transduced them with DNA encoding for TPC2-Cherry using lentivirus. Live primary MKs expressing TPC2-Cherry were incubated with mepacrine, the gold standard for PDG staining (Reddington *et al.*, 1987), and imaged by confocal fluorescence microscopy. TPC2-Cherry showed a high degree of colocalization with mepacrine (MOC = 0.65 ± 0.09), indicating that exogenously expressed TPC2 also localizes to PDGs in primary MKs (Figure 2A). To detect endogenous TPC2, we raised chicken affinity-purified polyclonal antibodies against TPC2. As seen by immunoblotting analysis, the antibodies recognized a band of the expected molecular weight in cell extracts (Supplemental Figure S2A). Confirmation that the antibodies recognized endogenous TPC2 protein was obtained by parallel immunoblotting experiments using extracts from cells subjected to TPC2 knockdown with two independent small interfering RNA (siRNA) oligonucleotides (Supplemental Figure S2, A and B). The chicken antibodies were used to label endogenous TPC2 in thin sections of primary MKs subjected to immunogold electron microscopy (Figure 2B and Supplemental Figure S3). Electron micrographs showed that although labeling efficiency was low, TPC2 essentially localized to PDGs and immature PDGs/late endosomes (62 and 26% of the label, respectively; 192 gold particles, 12 cells; Figure 2B and Supplemental Figure S3). To complement our microscopy studies, we carried out a subcellular fractionation of primary MKs. A postnuclear supernatant obtained from a primary MK total extract was subjected to a 10–60% linear sucrose gradient. We previously determined that under the experimental conditions used here, fraction 9 contains the most mature PDGs, fractions 7 and 8 contain immature PDGs, and fractions 1 and 2 contain small vesicles and cytosolic components (Ambrosio *et al.*, 2012). Consistently, the mature PDG marker ADP was found in fraction 9 in addition to fractions 1 and 2, which correspond to cytosolic ADP (Figure 2C). Immunoblotting analysis showed the presence of TPC2 in fractions 8 and 9, corroborating that TPC2 is a component of PDGs (Figure 2C). A cohort of TPC2 is present in fractions 1 and 2, likely representing small vesicles as previously observed for the PDG component LAMP2 (Ambrosio *et al.*, 2012). Further, immunomagnetic isolation of organelles containing endogenous TPC2 with an anti-TPC2 antibody from MEG-01 cells showed the presence of the PDG marker LAMP2, as determined by immunoblotting (Supplemental Figure S2C).

We previously reported that vesicular transport of a PDG integral membrane protein, VMAT2, depends on a dileucine-based sorting signal present in its cytosolic tail (Ambrosio *et al.*, 2012). TPC2 contains a sequence conforming to the dileucine-based signal consensus in its amino-terminal cytosolic tail. Mutation of the corresponding amino acid residues (LL11-12AA) caused mistargeting of the protein to the plasma membrane of human MEG-01 cells,

indicating a severe transport defect (Supplemental Figure S4). Thus, similar to other PDG integral membrane proteins, transport of TPC2 to PDGs relies on a dileucine-based sorting signal.

TPC2 overexpression results in alkalization of PDG lumen

TPC2 has been proposed as a Ca^{2+} release channel (Calcraft *et al.*, 2009). Ca^{2+} and H^+ movement across membranes of acidic organelles is believed to be coupled by Ca^{2+}/H^+ exchanger systems that rapidly bring Ca^{2+} back inside the compartment in exchange for protons going out (Patel and Docampo, 2010). To investigate the effect of TPC2 on the PDG lumen pH, we engineered a genetically encoded ratiometric pH sensor named tandem-fluorescence LAMP2 (tfLAMP2). Enhanced GFP (EGFP) and monomeric red fluorescent protein (mRFP) were cloned in tandem at the N-terminus of LAMP2, resulting in the expression of both fluorescent proteins inside the PDG (Figure 3A). In contrast to mRFP, EGFP fluorescence is quenched at low pH. Consequently, the ratio between red and green fluorescence intensities can be used to record changes in PDG luminal pH. MEG-01 cells expressing tfLAMP2 and incubated in buffers with pH values ranging from 4 to 7.2 showed that the red/green ratio is proportional to the pH of the buffers up to pH 6 (Supplemental Figure S5). Using this calibration curve as a reference, we calculated the luminal pH of PDGs from control live cells as 5.4, in accordance with the previously reported value. Cells treated with the proton pump inhibitor BafA1 showed an increase in PDG luminal pH (≥6.0), demonstrating the power of this tool to detect pH changes in PDGs (Supplemental Figure S5).

Mutation of a leucine residue in the TPC2 pore (L265P) impairs Ca^{2+} release by the channel (Brailoiu *et al.*, 2009, 2010; Lu *et al.*, 2013). MEG-01 cells were transfected with wild-type (wt) or L265P TPC2 tagged with an infrared fluorescent protein (iRFP) together with tfLAMP2 as pH reporter. tfLAMP2 and TPC2-iRFP displayed a high degree of colocalization (MOC = 0.56 ± 0.02). Cells coexpressing wt TPC2-iRFP and tfLAMP2 displayed a lower red/green fluorescence intensity ratio than cells expressing the pH reporter alone, indicating that overexpression of TPC2 significantly increased the luminal pH of PDGs (Figure 3). Of importance, the pore mutant L265P TPC2-iRFP causes a significantly less pronounced luminal pH increase than wt TPC2-iRFP, indicating that ion flux though TPC2 is required to achieve this effect (Figure 3).

Both TPC2 knockdown and pharmacological inhibition of Ca^{2+} release result in PDG lumen acidification

As an additional approach to determine changes in the pH of PDGs in live cells, we used mNectarine (Johnson *et al.*, 2009). First, we cloned mNectarine at the N-terminus of LAMP2 in order to localize the biosensor inside PDGs and validated its use in MEG-01 cells (Supplemental Figure S6, A and B). We then used mNectarine-LAMP2 to study the effect of TPC2 overexpression or knockdown on PDG luminal pH. MEG-01 cells were transfected with mNectarine-LAMP2 alone or together with TPC2-GFP. Cells overexpressing TPC2-GFP showed luminal PDG alkalization, as indicated by the increase in mNectarine-LAMP2 fluorescence intensity (Figure 4, A and B). The opposite effect was observed when TPC2 was knocked down by means of two different TPC2 siRNAs. Cells treated with both TPC2 siRNA1 and siRNA2 displayed a marked reduction of mNectarine-LAMP2 fluorescence intensity, showing the acidification of PDGs and demonstrating that the level of TPC2 expression regulates PDG luminal pH (Figure 4, A and B).

In nonspecialized cells, the NAADP antagonist Ned19 blocked Ca^{2+} release from acidic organelles, presumably by inhibiting TPC2 (Lu *et al.*, 2013). We investigated the effect of blocking Ca^{2+} release on both luminal PDG free Ca^{2+} and luminal PDG pH. MEG-01 cells expressing mNectarine-LAMP2 were subjected to loading of their PDGs with a membrane-impermeant version of the green fluorescent Ca^{2+} indicator Fluo3, followed by a 4-h chase period (Figure 4, C and D). Fluorescence microscopy analysis showed that Ned19-treated cells displayed the expected increase in PDG luminal free Ca^{2+} as determined by the rise in Fluo3 fluorescence intensity. The impairment in Ca^{2+} release from PDGs caused by Ned19 treatment also resulted in acidification of PDGs, as noted by a decrease in mNectarine-LAMP2 fluorescence intensity. Similarly, cells treated with TPC2 siRNA1 showed an increase in Fluo3 fluorescence intensity and decrease in mNectarine fluorescence intensity relative to cells treated with control siRNA, demonstrating an increase in luminal PDG free Ca^{2+} and acidification of PDGs (Supplemental Figure S6C). Together these results are in agreement with previous observations that NAADP/TPCs induce alkalization of acidic organelles (Cosker *et al.*, 2010; Morgan *et al.*, 2015). In addition, these data support a model in which TPC2 mediates Ca^{2+} release from PDGs followed by Ca^{2+} reuptake in exchange for H^+, thus increasing pH in the PDG lumen (Morgan *et al.*, 2015). Alternatively, the fact that TPC1 was shown to be permeant to H^+ offers a new explanation for the increased in luminal pH of acidic organelles induced by some TPCs (Pitt *et al.*, 2014).

TPC2 regulates the formation of Ca^{2+} nanodomains around PDGs that precisely mark organelle "kiss-and-run" events

To study directly a function of TPC2 in Ca^{2+} release from PDGs to the cytosol in live cells, we attached the genetically encoded Ca^{2+} sensor GCaMP6 (Chen *et al.*, 2013) directly to the C-terminal cytosolic tail of TPC2. The ability of TPC2-GCaMP6 to detect changes in Ca^{2+} levels on the cytosolic side of the PDG membrane in real time was tested by stimulating MEG-01 cells with thrombin or treating them with thapsigargin, an inhibitor of the sarcoplasmic/endoplasmic reticulum calcium ATPase family of Ca^{2+} ATPases that pumps Ca^{2+} from the cytosol into the dense tubular system/endoplasmic reticulum. Supplemental Figure S7 and Supplemental Video S1 show that TPC2-GCaMP6 fluorescence intensity changed dramatically in response to variations in cytosolic free Ca^{2+}.

Luminal Ca^{2+} release is believed to play a role in membrane fusion events with organelles of the endolysosomal system (Peters and Mayer, 1998; Luzio *et al.*, 2007). For example, Ca^{2+} nanodomains may form at organelle contact sites during "kiss-and-run" events. However, no visualization of such Ca^{2+} nanodomains in live cells has been reported, and the underlying mechanism is unclear. Further, "kiss-and-run" events have never been observed for PDGs. Here we transfected MEG-01 cells with TPC2 tagged with either GFP or GCaMP6 and performed confocal time-lapse imaging. In both cases, we observed organelle contact events between PDGs. However, only in cells expressing TPC2-GCaMP6 did we visualize the green protein lightening up in contact regions revealing the formation of Ca^{2+} nanodomains (Figure 5A). Line scans from representative examples showed that in cells expressing TPC2-GCaMP6, the fluorescence intensity in the contact region between PDGs is more than twice the intensity in the rest of the organelle (Figure 5B).

To study the dynamics of perigranular Ca^{2+} nanodomains, we followed PDG "kiss-and-run" events in MEG-01 cells coexpressing TPC2-GCaMP6 and the PDG marker VMAT2-Cherry (Figure 5C and Supplemental Video S2). Imaging in the red channel allowed tracking of PDGs at all times, and the green channel revealed sustained Ca^{2+} spikes when PDGs engaged in "kissing" events (see legend to Figure 5C for full description). These results indicate that TPC2-GCamP6 possesses appropriate sensitivity and kinetics to monitor the dynamics of perigranular Ca^{2+} nanodomains and its function in

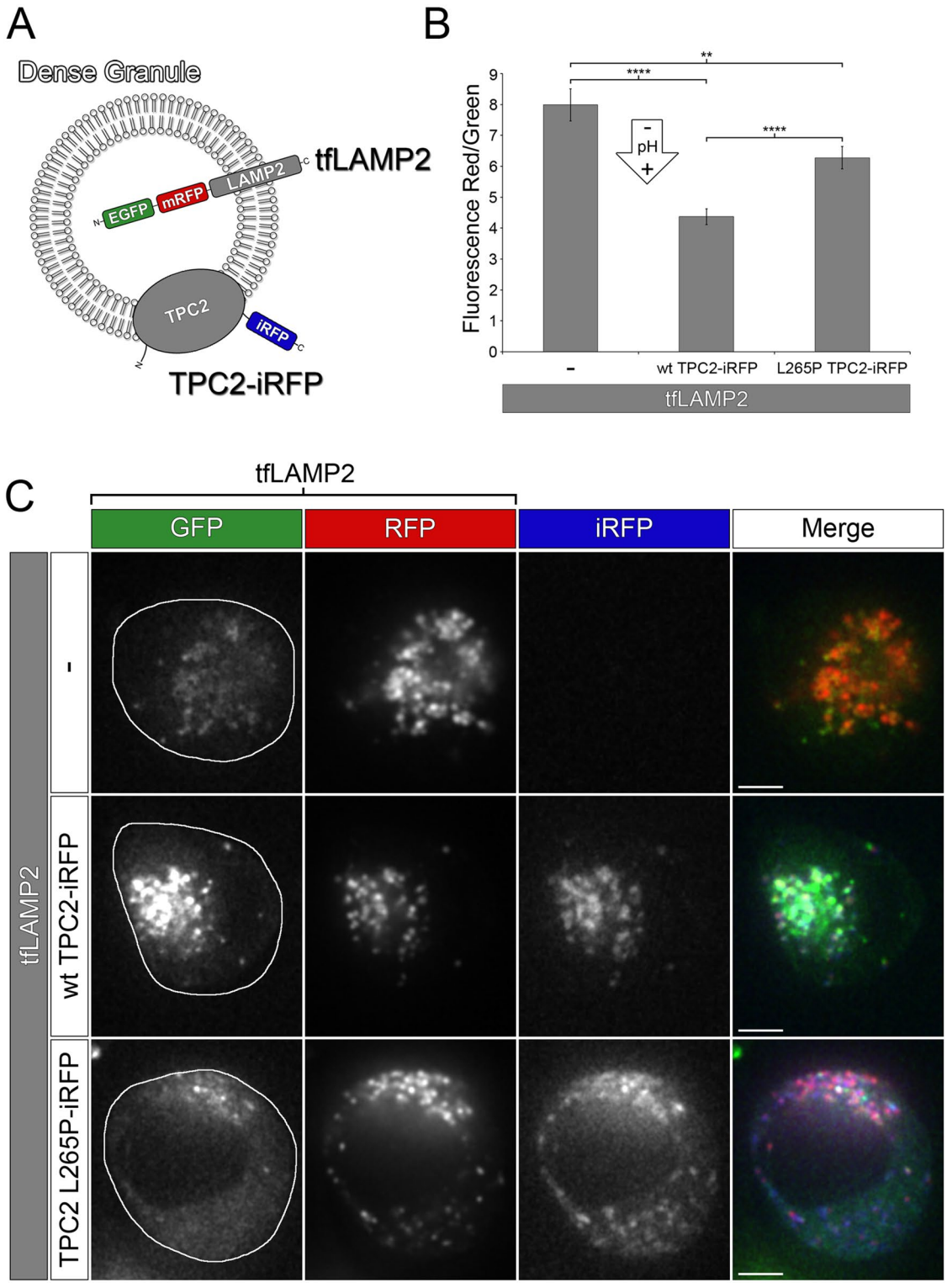

FIGURE 3: TPC2 overexpression alkalizes the lumen of PDGs. (A) Localization of fluorescent tags in PDG proteins. (B, C) Live MEG-01 cells expressing tf-LAMP2 alone or in combination with either wt TPC2-iRFP or the pore mutant L265P TPC2-iRFP were analyzed by spinning-disk confocal fluorescence microscopy. (B) The ratio between red and green fluorescence intensity as a measure of luminal pH was calculated for each treatment ($n \geq 56$ cells/treatment). A lower red/green fluorescence intensity ratio corresponds to higher pH. (C) Confocal fluorescence microscopy images of representative examples. Bar, 5 μm. iRFP, infrared fluorescent protein.

PDG membrane fusion events. Of importance, Ca^{2+} spikes around PDGs are visualized in real time for the first time and shown to precisely mark "kiss-and-run" events.

Is ion flux through TPC2 required for the formation of perigranular Ca^{2+} nanodomains? We compared cells expressing wt or L265P pore mutant TPC2-GCaMP6 together with VMAT2-Cherry

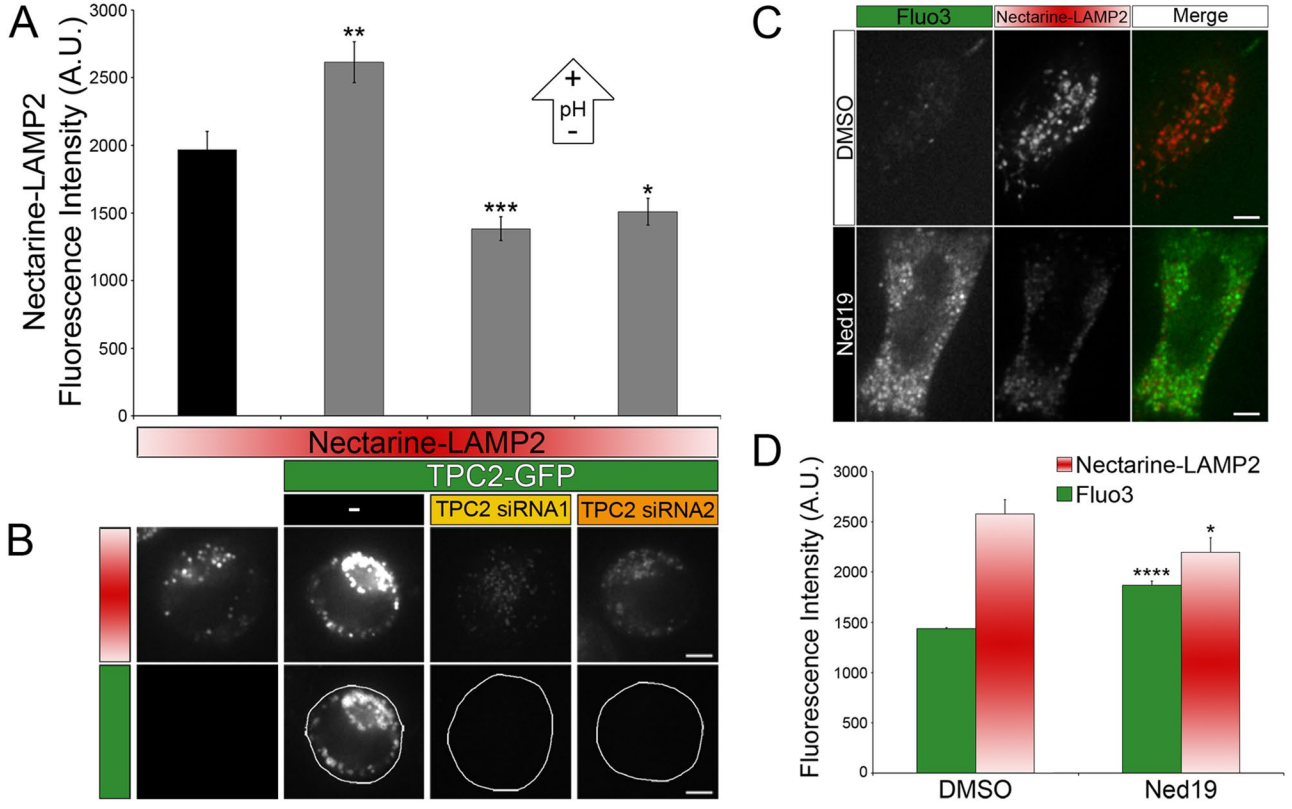

FIGURE 4: TPC2 knockdown or pharmacological inhibition acidify the lumen of PDGs. (A, B) MEG-01 cells expressing mNectarine-LAMP2 alone or in combination with wt TPC2-GFP and either an irrelevant siRNA (–) or two independent TPC2 siRNAs (the same siRNAs used in Supplemental Figure S2) were analyzed by spinning-disk confocal fluorescence microscopy. (A) The average mNectarine-LAMP2 fluorescence intensity was calculated for each treatment ($n \geq 60$ cells/treatment). For statistical analysis, all gray bars were compared against the mNectarine-LAMP2 black bar. A higher mNectarine fluorescence intensity corresponds to higher pH. (B) Representative examples. Bar, 5 µm. (C, D) MEG-01 cells expressing mNectarine-LAMP2 were subjected to PDG loading with the cell-impermeant green fluorescent Ca^{2+} indicator Fluo3, followed by a 4-h chase period. Cells were subsequently treated with Ned19 to block Ca^{2+} release from PDGs or vehicle (dimethyl sulfoxide). (C) Spinning-disk confocal fluorescence microscopy images of representative examples. Bar, 5 µm. (D) The average fluorescence intensity of Fluo3 and mNectarine-LAMP2 was calculated for each treatment as measure of relative PDG luminal free [Ca^{2+}] and pH, respectively ($n \geq 59$ cells/treatment).

to label PDGs. Published data and our results indicated the L265P mutation did not affect either expression or traffic of the protein when compared with the wild type (Supplemental Figure S8, A and B). On the other hand, the green mean fluorescence intensity of cells expressing wt TPC2-GCaMP6 was significantly higher than that from cells expressing the mutant TPC2-GCaMP6, indicating that TPC2 functions in Ca^{2+} release from PDGs (Supplemental Figure S8, C–E). Of importance, cells expressing wt TPC2-GCaMP6 displayed a much higher number of Ca^{2+} spikes at PDG contact sites than cells expressing the pore mutant (Figure 5, D and E). Quantification showed a ~40:1 ratio in the number of Ca^{2+} spikes per frame when cells expressing wt TPC2-GCaMP6 and L265P TPC2-GCaMP6 were compared. These results indicate that functional TPC2 is required both for the release of Ca^{2+} from PDGs and the formation of perigranular Ca^{2+} nanodomains during PDG "kiss-and-run" events. To confirm a function of endogenous TPC2 in the release of Ca^{2+} from PDGs, we analyzed MEG-01 cells treated with control siRNA or TPC2 siRNA1 and expressing LAMP2-GCaMP6 (localizing the Ca^{2+} sensor on the cytosolic side of the PDG membrane). The mean GCaMP6 fluorescence intensity was significantly lower in TPC2-knockdown cells, indicating a lower perigranular Ca^{2+} concentration (Supplemental Figure S6C). Quantification showed a ~28:1 ratio in the number of Ca^{2+} spikes per frame when cells subjected to control siRNA and TPC2 siRNA1 were compared. VMAT2-Cherry was analyzed as a control and showed no fluorescence intensity change in TPC2 siRNA1 cells compared with control siRNA–treated cells.

PDGs display membrane tubule connections that are promoted by TPC2

The presence of TPC2-labeled tubules connected with PDGs was evident in cells overexpressing wt TPC2-GCaMP6 or TPC2-Cherry (Figure 6, A and B). Whereas PDG-associated tubules are occasionally observed in control cells without TPC2 overexpression, they are detected more frequently in TPC2-overexpressing cells. Of importance, quantification of two independent experiments revealed that PDG-associated tubules were observed in 45% of cells expressing wt TPC2-Cherry but in only 10% of cells expressing L265P TPC2-Cherry, indicating that ion flux through TPC2 was required for tubule formation (Figure 6C). The tubules were very dynamic, typically connected two PDGs (Supplemental Videos S3 and S4), and sometimes displayed a beads-on-a-string morphology with beads consistent

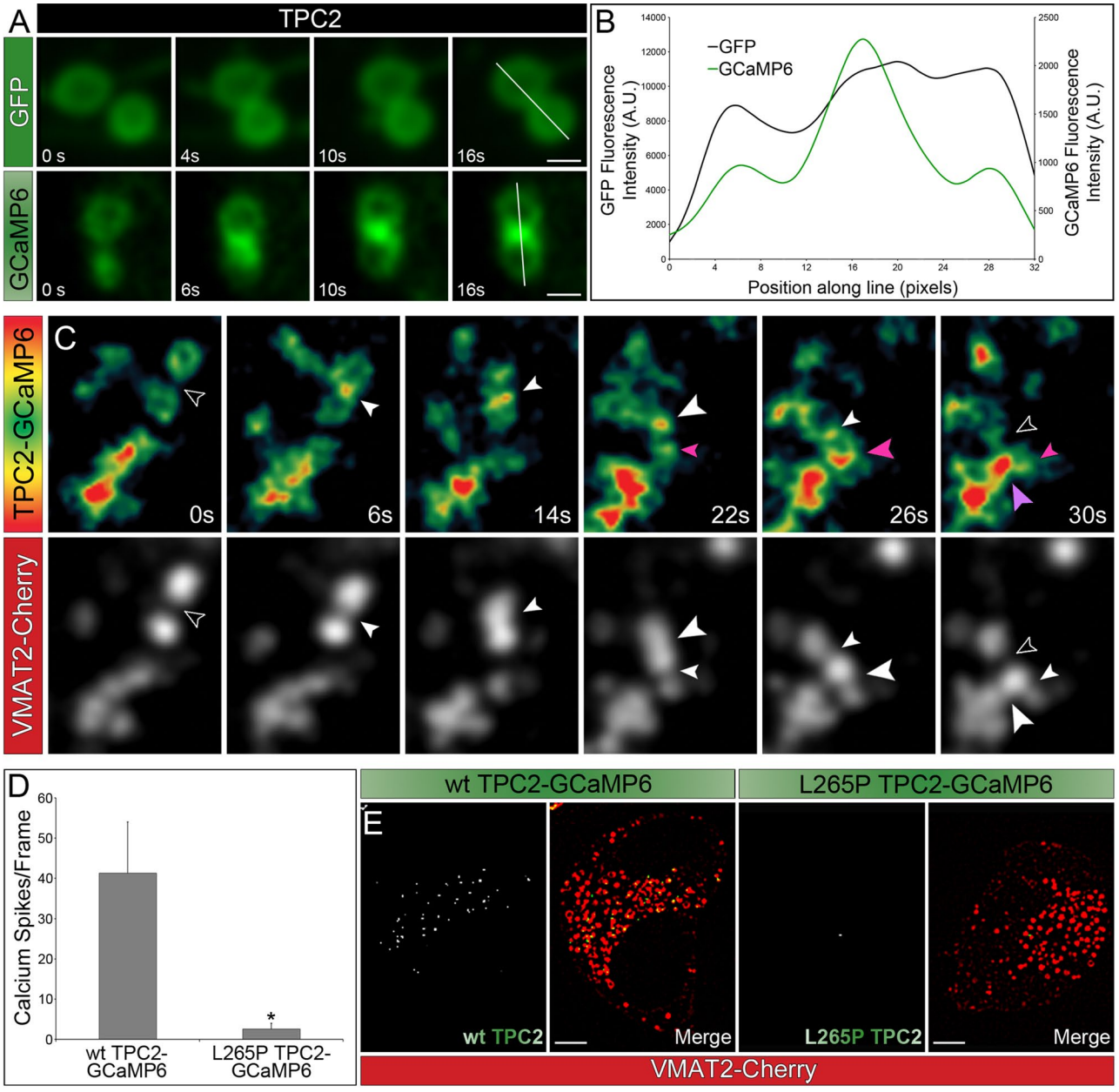

FIGURE 5: TPC2 mediates the formation of perigranular Ca^{2+} nanodomains. (A) Spinning-disk confocal fluorescence microscopy images at different time points of live MEG-01 cells expressing TPC2 tagged with either GFP or GCaMP6. Bar, 1 μm. (B) Fluorescence intensity line scans of the PDGs shown in A. (C) Spinning-disk confocal fluorescence microscopy images at different time points of MEG-01 cells coexpressing TPC2-GCaMP6 and VMAT2-Cherry. Top, heat maps based on the fluorescence intensity of TPC2-GCaMP6; bottom, the VMAT2-Cherry channel. Open arrowheads indicate no contact between PDGs. All other arrowheads indicate contact between PDGs; color and size of the arrowheads are used to compare contacts among different organelles. At time 0 s, the black arrowhead indicated the space between two PDGs that were not yet making contact (VMAT2-Cherry, bottom), and the TPC2-GCaMP6 heat map showed homogeneous fluorescence intensity around the organelles (top). Once these PDGs touched each other, a sustained Ca^{2+} spike was observed in the contact region (6–26 s, white arrowheads), which dissipated only when the PDGs moved away from each other (30 s, black arrowhead). At 22 s, another PDG was observed approaching and making contact with the mentioned pair and triggering a small Ca^{2+} spike (small pink arrow) that gained more intensity as the organelles got closer together (26 s, large pink arrow). Finally, the newly formed pair made contact with another granule, eliciting a large Ca^{2+} release (30 s, large purple arrow). (D, E) MEG-01 cells expressing wt TPC2-GCaMP6 or L265P TPC2-GCaMP6 and VMAT2-Cherry were analyzed. Ca^{2+} spikes were defined in Laplacian two-dimensional (2D) filtered confocal images as regions with GCaMP6 fluorescence intensity at least 1.02 times higher than background green fluorescence. (D) The average number of Ca^{2+} spikes per frame was calculated for wt and pore mutant TPC2 transfected cells. At least 30 frames/cell and 5 cells were used for each construct. (E) Laplacian 2D filtered confocal images of representative cells. Bar, 5 μm. See also Supplemental Figure S8.

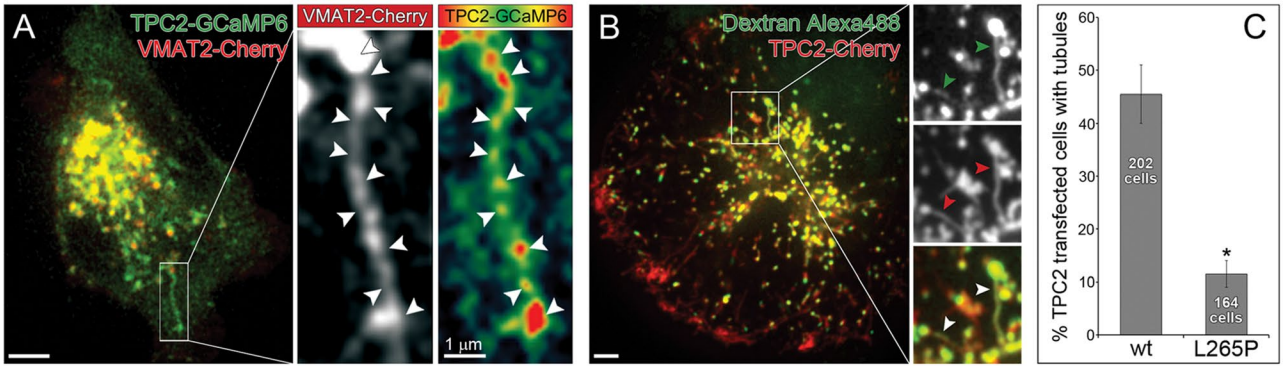

FIGURE 6: TPC2 promotes the formation of tubule connections between PDGs. (A) Spinning-disk confocal fluorescence microscopy image of a representative MEG-01 cell expressing wt TPC2-GCaMP6 and VMAT2-Cherry. Insets, magnified view of a TPC2- and VMAT2-labeled tubule. White arrowheads indicate Ca^{2+} spikes revealed by TPC2-GCaMP6 (intensity fluorescence map) that in most cases are intercalated between vesicles (VMAT2-Cherry image). Bar, 5 μm. (B) PDGs in a live MEG-01 cell expressing TPC2-cherry were loaded with the fluid- phase marker dextran–Alexa Fluor 488. Spinning-disk confocal fluorescence microscopy allows visualization of TPC2-labeled tubules. Insets show the presence of both dextran–Alexa Fluor 488 (green arrowheads) and TPC2-Cherry (red arrowheads) in the tubules. Bar, 5 μm. (C) The average percentage of cells with tubules was calculated for wt or L265P TPC2–expressing cells in two independent experiments.

with vesicle size (200- to 300-nm diffraction-limited puncta; Figure 6A, VMAT2-Cherry). Of interest, TPC2-GCaMP6 revealed Ca^{2+} spikes intercalated with the VMAT2-Cherry–labeled beads, suggesting that fusion of vesicles is what gives rise to the tubules (Figure 6A, TPC2-GCaMP6 intensity map). We reasoned that if Ca^{2+} spikes detected by TPC2-GCaMP6 represent membrane fusion events as a mechanism to form PDG-connecting tubules, then the lumen of these structures should be continuous and allow transfer of soluble content between them. MEG-01 cells transfected with TPC2-Cherry were subjected to PDG loading with the fluid-phase marker dextran–Alexa Fluor 488, a 4-h chase period, and confocal fluorescence microscopy analysis (Figure 6B). Fluorescent dextran was clearly observed in TPC2-Cherry–labeled PDGs and connecting tubules, indicating the existence of physical continuity and luminal transfer between PDGs. Tubules connecting PDGs were also observed in primary bone marrow MKs expressing TPC2-Cherry (Figure 2A, magnified inset, Supplemental Figure S9, and Supplemental Video S5). Moreover, incubation of primary MKs with the PDG-specific luminal dye mepacrine showed continuity between the lumen of PDGs and associated tubules (Figure 2A, magnified inset, Supplemental Figure S9, and Supplemental Video S5).

"Kiss-and-run" events and tubules mediate transfer of membrane proteins between PDGs

To investigate whether "kiss-and-run" events and tubule connections mediate direct transfer of membrane proteins between PDGs, we developed a photo/pulse-chase labeling strategy using LAMP2 tagged with photoactivatable GFP (LAMP2-PAGFP). The photo/pulse-chase assay was performed in live MEG-01 cells coexpressing the PDG markers VMAT2-Cherry and LAMP2-PAGFP (Figure 7, A–C, and Supplemental Video S6). Imaging with the red channel (VMAT2-Cherry) allowed tracking of PDGs over time. Immediately after a PDG was irradiated with 405-nm light for 10 ms, it displayed green fluorescence as a result of photoactivation of LAMP2-PAGFP molecules (Figure 7B). Note how PDGs that were not irradiated (observed in the red channel) remained undetectable in the green channel, demonstrating that photoactivation of the targeted PDG was precise (Figure 7B). Continuous tracking of the photoactivated PDG showed that it later contacted another PDG and engaged in "kiss-and-run" (Figure 7C). Of importance, the partner PDG developed green fluorescence, indicating that during the "kissing" event it acquired photoactivated LAMP2-PAGFP molecules from the irradiated PDG (Figure 7C). We also used the LAMP2-PAGFP photo/pulse-chase assay to investigate membrane protein transfer through PDG-associated tubules. We used MEG-01 cells coexpressing TPC2-Cherry, which both labels the tubules and enhances their formation (Figures 2A and 6). Figure 7, D and E, and Supplemental Video S7 (red channel, TPC2-Cherry) show the presence of two PDGs connected by a tubule. Irradiation of one of the PDGs caused photoactivation of its LAMP2-PAGFP molecules, which immediately became fluorescent. Continuous imaging in both channels showed that photoactivated LAMP2-PAGFP molecules quickly populate the tubule and then the second PDG connected by the tubule (Figure 7E). Together these experiments show that PDGs exchange material through a previously unknown mechanism, "kiss-and-run" events and tubule connections.

DISCUSSION

TPC2 was previously found in several acidic organelles (Calcraft *et al.*, 2009; Davis *et al.*, 2012; Wang *et al.*, 2012). Here we showed that TPC2 is a component of the PDG limiting membrane. In MEG-01 cells, TPC2-GFP colocalized with PDG markers LAMP2 and VMAT2, and immunogold electron microscopy analysis showed the presence of TPC2-GFP in PDGs. The coexistence of LAMP2 and TPC2 in the same organelles was confirmed by coimmunoprecipitation of the endogenous proteins from MEG-01 cell extracts. Of importance, localization of endogenous TPC2 to PDGs in primary MKs was determined by immunogold electron microscopy and subcellular fractionation. Further, TPC2-Cherry expressed in primary MKs localized to mepacrine-labeled compartments, demonstrating its presence in PDGs. Similar to VMAT2, TPC2 contains a dileucine-based sorting signal in its amino-terminal cytosolic tail needed for proper PDG targeting. Despite the importance of PDGs for platelet physiology, we know very little about the composition of their limiting membrane, and only a handful of proteins have been characterized.

Here TPC2 was established as a new component of the PDG membrane.

Although data from one laboratory differ in the ion selectivity (Wang *et al.*, 2012; Morgan and Galione, 2014), publications from several groups indicate that TPC2 functions in Ca^{2+} transport from acidic organelles to the cytosol (Calcraft *et al.*, 2009; Davis *et al.*, 2012; Lu *et al.*, 2013). Using a new approach, our data showed that TPC2 functions in Ca^{2+} release from PDGs. First, we observed higher cytosolic Ca^{2+} levels in cells expressing wt TPC2-GCamP6 than with the nonconducting pore mutant L265P TPC2-GCamP6. Second, we recorded 40 times more Ca^{2+} spikes around PDGs of cells expressing wt TPC2-GCaMP6 than cells expressing the pore mutant L265P TPC2. Similarly, we recorded 28 times more Ca^{2+} spikes around PDGs of control cells expressing LAMP2-GCaMP6 than in cells depleted for TPC2. Third, depletion of TPC2 or pharmacological inhibition by means of Ned19 to impede Ca^{2+} release from PDGs resulted in the same phenotype, PDG acidification, whereas overexpression of TPC2 had the opposite effect. Together our data strongly support TPC2 function in Ca^{2+} release from PDGs.

The connection between PDG luminal pH and Ca^{2+} and its regulation by TPC2 uncovered here has important implications for PDG function. PDGs contain polyphosphate, a linear polymer of P_i residues capable of binding Ca^{2+} and effectively acting as a Ca^{2+} buffer (Patel and Docampo, 2010). The protonation state of the polyphosphate is predicted to determine the amount of Ca^{2+} bound to this matrix; an increase in pH will cause more Ca^{2+} binding to the matrix and therefore lower free Ca^{2+} in the PDG lumen. This is important because free Ca^{2+} in the PDG lumen is needed for Ca^{2+} release to the cytosol. Supporting this model, we found that treatment with BafA1, which alkalizes PDGs, resulted in inhibition of Ca^{2+} release by PDGs (Supplemental Figure S10).

PDGs are believed to develop from late endosomes/multi vesicular bodies upon receiving newly synthesized membrane proteins such as the serotonin transporter VMAT2 through vesicular trafficking (Ambrosio *et al.*, 2012). This study revealed previously unknown PDG membrane dynamics: "kiss-and-run" events and tubule connections. These processes provide a mechanism for exchange of both membrane and soluble components between PDGs and likely play a role in PDG maturation. Through "kiss-and-run" events and connecting tubules, the PDG population could achieve homogenization or segregation of membrane and luminal contents, as well as regulation of organelle volume. Thus our results uncovered a new layer in the mechanism of PDG biogenesis that is regulated by TPC2 and likely operates in addition to vesicular trafficking.

"Kiss-and-run" events and tubule connections rely on membrane fusion. The involvement of luminal Ca^{2+} release as a postdocking event required for membrane fusion between other organelles of the endolysosomal system was first reported in yeast using in vitro reconstitution assays (Peters and Mayer, 1998). However, to our knowledge, this is the first time that Ca^{2+} spikes around PDGs (or other organelles of the endolysosomal family) have been visualized in live cells in real time. Of importance, our approach revealed that Ca^{2+} nanodomains exquisitely mark PDG contact sites during "kiss-and-run" events. Ca^{2+} spikes also occur along forming PDG tubular connections, suggesting that tubules are generated at least in part by the fusion of vesicles. Mechanistically, results with wt and L265P TPC2-GCaMP6 show that TPC2 regulates Ca^{2+} release from PDGs to mediate "kiss-and-run" events and tubule formation. Of interest, physical interactions between TPC2 and Rab and soluble *N*-ethylmaleimide–sensitive factor attachment protein receptor (SNARE) proteins Rab7 and STX7 and additional components of SNARE complexes were recently reported in nonspecialized cells (Grimm *et al.*, 2014; Lin-Moshier *et al.*, 2014). Thus TPC2 is linked to the endolysosome tethering and fusion machinery. In MKs, TPC2 may interact with PDG-specific Rabs and SNARE proteins during PDG biogenesis (Ren *et al.*, 2008; Graham *et al.*, 2009). Our results predict that TPC2 deficiency would affect platelet function due to defective PDG biogenesis and function. A role for TPC2 in platelet physiology is further supported by the fact that the agonist NAADP and inhibitor Ned19 regulate human platelet function. Specifically, NAADP was found to trigger Ca^{2+} release from intracellular stores and Ned19 to inhibit thrombin-induced Ca^{2+} release in human platelets. Of importance, Ned19 inhibited platelet aggregation and extended clotting time in whole-blood samples (Coxon *et al.*, 2012). Because TPC2 polymorphisms underlie pigmentation variations in humans, TPC2 deficiency could cause Hermansky–Pudlak syndrome. It will be important to investigate these possibilities.

MATERIALS AND METHODS

Expression vectors

The cDNAs for VMAT2—Rab7a, Rab5a, LAMP2A, TPC1, and TPC2—were amplified from total RNA of human MEG-01 cells by reverse transcriptase-PCR and cloned into pmCherry. TPC2 cDNA was subcloned into pEGFP, pGP-CMV-GCaMP6m (40754; Addgene; Chen *et al.*, 2013), and piRFP682-N1 (45459; Addgene; Shcherbakova and Verkhusha, 2013). Site-directed mutagenesis was performed with QuikChange II Kit (Agilent Technologies, Santa Clara, CA). LAMP2A was cloned into pBAD-mNectarine (21717; Addgene; Johnson *et al.*, 2009), pGP-CMV-GCaMP6m, and pPAGFP (18697; Addgene). tfLAMP2 was made by introducing mRFP and LAMP2A cDNAs downstream from EGFP in a pEGFP-C2 vector. Constructs were verified by DNA sequencing.

Antibodies

TPC2-C antibody was generated by immunizing chickens with purified recombinant histidine (His)-TPC2-695-752 fragment and affinity purified with the His-TPC2 fragment covalently coupled to Affi-Gel 15 beads (Bio-Rad, Hercules, CA). Rabbit TPCN2 antibody was from Sigma-Aldrich (St. Louis, MO). Horseradish peroxidase–conjugated secondary antibodies were from GE Amersham (Pittsburgh, PA). Colloidal gold–complexed secondary antibodies (18 nm) were from Jackson ImmunoResearch (West Grove, PA).

Cell culture

Human MEG-01 cell culture, transfection, siRNA treatment, and mouse bone marrow MK isolation were performed as described (Leven, 2004; Ambrosio *et al.*, 2012). Oligonucleotides (Sigma-Aldrich) used for siRNA were as follows: negative control (SIC001-10 NMOL), TPC2 siRNA1 (SASI_Hs01_00129376), and TPC2 siRNA2 (SASI_Hs01_00129381). For dextran or Fluo3 uptake experiments, cells were incubated for 16 h at 37°C in medium containing 250 µg/ml dextran-Alexa Fluor 488 or 3 µM Fluo3 (Molecular Probes, Eugene, OR), followed by a 4-h chase period. We previously determined that soluble tracers such as dextran taken up by endocytosis accumulate in PDGs (Ambrosio *et al.*, 2012). Mepacrine was added to the medium (10 µM), followed by a 5-min incubation at 37°C.

Production of TCP2-Cherry–expressing lentiviruses

The TCP2-Cherry cDNA was cloned into pLKO.1 (Sigma-Aldrich), replacing the puromycin resistance gene. The resulting plasmid was cotransfected with a third-generation lentivirus packaging mix (K4975-00; Life Technologies, Carlsbad, CA) into HEK293T cells by

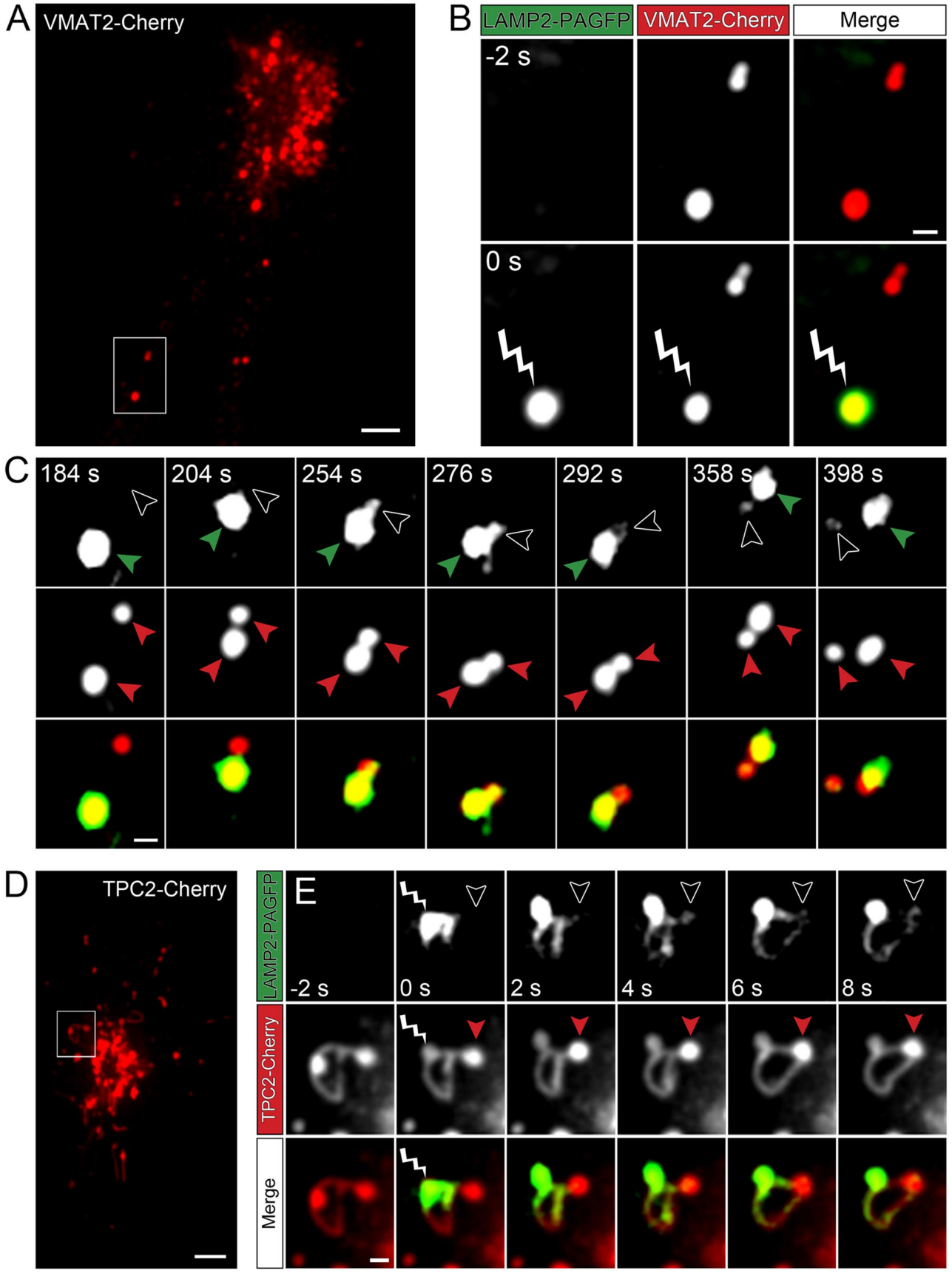
A
VMAT2-Cherry
B
LAMP2-PAGFP
VMAT2-Cherry
Merge
-2 s
0 s
C
184 s
204 s
254 s
276 s
292 s
358 s
398 s
D
TPC2-Cherry
E
LAMP2-PAGFP
TPC2-Cherry
Merge
-2 s
0 s
2 s
4 s
6 s
8 s

FIGURE 7: "Kiss-and-run" events and tubule connections mediate transfer of membrane proteins between PDGs. (A) MEG-01 cells expressing VMAT2-Cherry and LAMP2-PGFP were analyzed by spinning-disk confocal fluorescence microscopy. A frame of the video 2 s before photoactivation of a selected PDG. The highlighted area shows two PDGs, one of which is subsequently photoactivated. Bar, 5 µm. (B) Magnified view of the area highlighted in A shown 2 s before (-2 s) and immediately after (0 s) irradiation of a selected PDG with 405-nm light for 10 ms. The irradiated PDG is identified with a lightning bolt symbol, and photoactivation is evidenced by the immediate development of intense green fluorescence. Bar, 1 µm. (C) The PDG subjected to photoactivation in B was tracked over time and observed to engage in "kiss-and-run" activity with a second PDG (not photoactivated). Top, green channel (photoactivated LAMP-2-PAGFP); middle, red channel (VMAT2-Cherry); bottom, overlay. Red arrowheads track both PDGs at all times in the red channel. In the green channel, green arrowheads track the photoactivated PDG and open arrowheads indicate the second PDG that approaches and engages in "kiss-and-run" with the photoactivated PDG. Note the appearance of green fluorescence in the nonphotoactivated PDG (open arrowhead) starting at frame 254 s as a result of the "kiss." The PDGs separate from each other ("run") by frame 398 s. (D) MEG-01 cells expressing TPC2-Cherry and LAMP2-PAGFP were analyzed by spinning-disk confocal fluorescence microscopy. A frame of the video 2 s before photoactivation of a selected PDG. The highlighted area shows two PDGs connected by a tubule, one of which is subsequently photoactivated. Bar, 5 µm. (E) Magnified view of the area highlighted in D shown 2 s before (-2 s), immediately after (0 s), and at various time intervals after irradiation of a selected PDG with 405-nm light for 10 ms. The irradiated PDG is identified with a lightning bolt symbol, and photoactivation is evidenced by the immediate development of intense green fluorescence. Note that photoactivated LAMP2-PAGFP molecules quickly populate the connecting tubule and then the second PDG (indicated at all times with an open arrowhead in the green channel and a red arrowhead in the red channel). Bar, 1 µm.

calcium phosphate as previously described (Huang and Chen, 2010). After ~48 h, the culture medium was collected, filtered through a 0.45-µm filter, and concentrated by >20-fold with a 100-kDa–cut-off Amicon Ultra concentrator (Millipore, Billerica, MA).

Fluorescence and electron microscopy

Cells were imaged as previously described (Ambrosio *et al.*, 2012) using a temperature- controlled chamber at 37°C and 5% CO_2 on an Olympus IX81 spinning-disk confocal microscope with Photometrics Cascade II camera, a 100×/1.40 numerical aperture objective, and phasor holographic photobleaching/photoactivation system (Intelligent Imaging Innovations [3i], Denver, CO). Excitation was performed with diode lasers of 473 nm (GFP, GCaMP6, mepacrine, and dextran–Alexa Fluor 488), 561 nm (mCherry, mNectarine), and 658 nm (iRFP). The microscope has a CSU 22 head with quad dichroic and additional emission filter wheel to eliminate spectral crossover. The following emission filters were used: 521 ± 12.5, 607 ± 12.5, and 700 ± 12.5 nm. Images and videos were acquired and analyzed with SlideBook 5.5 software (3i). The colocalization module with autothreshold was used to determine the MOC of two-color images processed with a Laplacian two-dimensional filter. High-pressure freezing, fixation, immunogold labeling, and electron microscopy were performed as described (Ambrosio *et al.*, 2012).

Biochemical procedures

Primary mouse MK postnuclear supernatant was prepared and fractionated using a 12-ml linear sucrose gradient (10–60%) as described (Ambrosio *et al.*, 2012). Fractions of 1 ml were collected and used for immunoblotting and ADP determination using the Enzylight ADP bioluminescence assay kit (BioAssay Systems, Hayward, CA). For immunoblotting, proteins were fractionated on precast 4–20% gradient SDS/polyacrylamide gels (Life Technologies) and transferred by electroblotting to polyvinylidene fluoride membranes. Membranes were incubated sequentially with blocking buffer, primary antibody, and horseradish peroxidase–conjugated secondary antibody as described (Nazarian *et al.*, 2006). Bound antibodies were detected by using ECL Prime Western blotting reagent (GE Amersham, Pittsburgh, PA). Immunoprecipitations were carried out using protein G magnetic beads (Life Technologies) and 2 µg of the appropriate antibody.

RNA analysis

Total RNA from MEG-01 control and siRNA-treated cells was isolated 24 h after transfection using the Aurum Total RNA Mini Kit (Bio-Rad) following the manufacturer's instructions. A 500-ng amount of purified RNA was used in reverse-transcription reactions using the iScript cDNA synthesis kit (Bio-Rad). Relative amounts of each transcript were determined in duplicate by real-time PCR using gene-specific primers (forward, TGCATATCGGCGCTACTCAG; reverse, AGTCATCTGGTAGGTGGCCT) and normalized against glyceraldehyde-3-phosphate dehydrogenase mRNA (forward, TGTTGCCATCAATGACCCCT; reverse, TCGCCCCACTTGATTTTGGA).

Statistical analysis

Details on statistical analysis and *n* values are provided in the figure legends. Error bars indicate mean ± SEM. Statistical significance was determined via Student's *t* test: $*p \le 0.05$; $**p \le 0.01$; $***p \le 0.001$; $****p \le 0.0001$.

ACKNOWLEDGMENTS

We thank Thomas Giddings for help with high-pressure freezing and electron microscopy and Chaoping Chen for lentivirus packaging. This work was supported by National Institutes of Health Grant R01HL106186 to S.M.D. Microscopes were supported in part by a Colorado State University Microscope Imaging Network Core Infrastructure Grant.

REFERENCES

Ambrosio AL, Boyle JA, Di Pietro SM (2012). Mechanism of platelet dense granule biogenesis: study of cargo transport and function of Rab32 and Rab38 in a model system. Blood 120, 4072–4081.

Brailoiu E, Churamani D, Cai X, Schrlau MG, Brailoiu GC, Gao X, Hooper R, Boulware MJ, Dun NJ, Marchant JS, Patel S (2009). Essential requirement for two-pore channel 1 in NAADP-mediated calcium signaling. J Cell Biol 186, 201–209.

Brailoiu E, Rahman T, Churamani D, Prole DL, Brailoiu GC, Hooper R, Taylor CW, Patel S (2010). An NAADP-gated two-pore channel targeted to the plasma membrane uncouples triggering from amplifying Ca2+ signals. J Biol Chem 285, 38511–38516.

Broos K, Feys HB, De Meyer SF, Vanhoorelbeke K, Deckmyn H (2011). Platelets at work in primary hemostasis. Blood Rev 25, 155–167.

Calcraft PJ, Ruas M, Pan Z, Cheng X, Arredouani A, Hao X, Tang J, Rietdorf K, Teboul L, Chuang KT, *et al.* (2009). NAADP mobilizes calcium from acidic organelles through two-pore channels. Nature 459, 596–600.

Carty SE, Johnson RG, Scarpa A (1981). Serotonin transport in isolated platelet granules. Coupling to the electrochemical proton gradient. J Biol Chem 256, 11244–11250.

Chen TW, Wardill TJ, Sun Y, Pulver SR, Renninger SL, Baohan A, Schreiter ER, Kerr RA, Orger MB, Jayaraman V, *et al.* (2013). Ultrasensitive fluorescent proteins for imaging neuronal activity. Nature 499, 295–300.

Cosker F, Cheviron N, Yamasaki M, Menteyne A, Lund FE, Moutin MJ, Galione A, Cancela JM (2010). The ecto-enzyme CD38 is a nicotinic acid adenine dinucleotide phosphate (NAADP) synthase that couples receptor activation to Ca2 +mobilization from lysosomes in pancreatic acinar cells. J Biol Chem 285, 38251–38259.

Coxon CH, Lewis AM, Sadler AJ, Vasudevan SR, Thomas A, Dundas KA, Taylor L, Campbell RD, Gibbins JM, Churchill GC, Tucker KL (2012). NAADP regulates human platelet function. Biochem J 441, 435–442.

Davis LC, Morgan AJ, Chen JL, Snead CM, Bloor-Young D, Shenderov E, Stanton-Humphreys MN, Conway SJ, Churchill GC, Parrington J, *et al.* (2012). NAADP activates two-pore channels on T cell cytolytic granules to stimulate exocytosis and killing. Curr Biol 22, 2331–2337.

Flaumenhaft R (2012). Platelet secretion. In: Platelets, ed. AD Michelson, Waltham, MA: Academic Press, 343–366.

Graham GJ, Ren Q, Dilks JR, Blair P, Whiteheart SW, Flaumenhaft R (2009). Endobrevin/VAMP-8-dependent dense granule release mediates thrombus formation in vivo. Blood 114, 1083–1090.

Grimm C, Hassan S, Wahl-Schott C, Biel M (2012). Role of TRPML and two-pore channels in endolysosomal cation homeostasis. J Pharmacol Exp Ther 342, 236–244.

Grimm C, Holdt LM, Chen CC, Hassan S, Muller C, Jors S, Cuny H, Kissing S, Schroder B, Butz E, *et al.* (2014). High susceptibility to fatty liver disease in two-pore channel 2-deficient mice. Nat Commun 5, 4699.

Holmsen H, Weiss HJ (1979). Secretable storage pools in platelets. Annu Rev Med 30, 119–134.

Huang L, Chen C (2010). Autoprocessing of human immunodeficiency virus type 1 protease miniprecursor fusions in mammalian cells. AIDS Res Ther 7, 27.

Huizing M, Helip-Wooley A, Westbroek W, Gunay-Aygun M, Gahl WA (2008). Disorders of lysosome-related organelle biogenesis: clinical and molecular genetics. Annu Rev Genomics Hum Genet 9, 359–386.

Johnson DE, Ai HW, Wong P, Young JD, Campbell RE, Casey JR (2009). Red fluorescent protein pH biosensor to detect concentrative nucleoside transport. J Biol Chem 284, 20499–20511.

Leven RM (2004). Isolation of primary megakaryocytes and studies of proplatelet formation. Methods Mol Biol 272, 281–291.

Lin-Moshier Y, Keebler MV, Hooper R, Boulware MJ, Liu X, Churamani D, Abood ME, Walseth TF, Brailoiu E, Patel S, Marchant JS (2014). The two-pore channel (TPC) interactome unmasks isoform-specific roles for TPCs in endolysosomal morphology and cell pigmentation. Proc Natl Acad Sci USA 111, 13087–13092.

Lu Y, Hao BX, Graeff R, Wong CW, Wu WT, Yue J (2013). Two pore channel 2 (TPC2) inhibits autophagosomal-lysosomal fusion by alkalinizing lysosomal pH. J Biol Chem 288, 24247–24263.

Luzio JP, Bright NA, Pryor PR (2007). The role of calcium and other ions in sorting and delivery in the late endocytic pathway. Biochem Soc Trans 35, 1088–1091.

McNicol A, Israels SJ (1999). Platelet dense granules: structure, function and implications for haemostasis. Thromb Res 95, 1–18.

Meng R, Wang Y, Yao Y, Zhang Z, Harper DC, Heijnen HF, Sitaram A, Li W, Raposo G, Weiss MJ, *et al.* (2012). SLC35D3 delivery from megakaryocyte early endosomes is required for platelet dense granule biogenesis and is differentially defective in Hermansky-Pudlak syndrome models. Blood 120, 404–414.

Morgan AJ, Davis LC, Ruas M, Galione A (2015). TPC: the NAADP discovery channel?. Biochem Soc Trans 43, 384–389.

Morgan AJ, Galione A (2014). Two-pore channels (TPCs): current controversies. Bioessays 36, 173–183.

Nazarian R, Starcevic M, Spencer MJ, Dell'Angelica EC (2006). Reinvestigation of the dysbindin subunit of BLOC-1 (biogenesis of lysosome-related organelles complex-1) as a dystrobrevin-binding protein. Biochem J 395, 587–598.

Patel S, Docampo R (2010). Acidic calcium stores open for business: expanding the potential for intracellular Ca2+ signaling. Trends Cell Biol 20, 277–286.

Peters C, Mayer A (1998). Ca2+/calmodulin signals the completion of docking and triggers a late step of vacuole fusion. Nature 396, 575–580.

Pitt SJ, Lam AK, Rietdorf K, Galione A, Sitsapesan R (2014). Reconstituted human TPC1 is a proton-permeable ion channel and is activated by NAADP or Ca2+. Sci Signal 7, ra46.

Reddington M, Novak EK, Hurley E, Medda C, McGarry MP, Swank RT (1987). Immature dense granules in platelets from mice with platelet storage pool disease. Blood 69, 1300–1306.

Ren Q, Ye S, Whiteheart SW (2008). The platelet release reaction: just when you thought platelet secretion was simple. Curr Opin Hematol 15, 537–541.

Shcherbakova DM, Verkhusha VV (2013). Near-infrared fluorescent proteins for multicolor in vivo imaging. Nat Methods 10, 751–754.

Thon JN, Italiano JE (2012). Platelets: production, morphology and ultrastructure. Handb Exp Pharmacol 2012, 3–22.

Wang X, Zhang X, Dong XP, Samie M, Li X, Cheng X, Goschka A, Shen D, Zhou Y, Harlow J, *et al.* (2012). TPC proteins are phosphoinositide-activated sodium-selective ion channels in endosomes and lysosomes. Cell 151, 372–383.

Youssefian T, Cramer EM (2000). Megakaryocyte dense granule components are sorted in multivesicular bodies. Blood 95, 4004–4007.

Zhu MX, Ma J, Parrington J, Calcraft PJ, Galione A, Evans AM (2010). Calcium signaling via two-pore channels: local or global, that is the question. Am J Physiol Cell Physiol 298, C430–C441.